Dynamical nucleus-nucleus potential at short distances

Yongying Jiang,[1] Ning Wang,[1,*] Zhuxia Li,[2] and Werner Scheid[3]
[1]*Department of Physics, Guangxi Normal University, Guilin 541004, People's Republic of China*
[2]*China Institute of Atomic Energy, Beijing 102413, People's Republic of China*
[3]*Institute for Theoretical Physics, Justus-Liebig-University, D-35392 Giessen, Germany*
(Received 2 December 2009; published 2 April 2010)

The dynamical nucleus-nucleus potentials for fusion reactions $^{40}Ca + ^{40}Ca$, $^{48}Ca + ^{208}Pb$, and $^{126}Sn + ^{130}Te$ are studied with the improved quantum molecular dynamics model together with the extended Thomas-Fermi approximation for the kinetic energies of nuclei. The obtained fusion barrier for $^{40}Ca + ^{40}Ca$ is in good agreement with the extracted fusion barrier from the measured fusion excitation function, and the depths of the fusion pockets are close to the results of time-dependent Hartree-Fock calculations. The energy dependence of the fusion barrier is also investigated. The fusion pocket becomes shallow for a heavy fusion system and almost disappears for heavy nearly symmetric systems, and the obtained potential at short distances is higher than the adiabatic potential.

DOI: 10.1103/PhysRevC.81.044602 PACS number(s): 25.70.Jj

I. INTRODUCTION

The synthesis of superheavy elements has been studied for many years both theoretically and experimentally [1–4]. Up to now superheavy nuclei have been uniquely synthesized through fusion reactions, including "cold" fusion reactions with lead and bismuth targets [3] and "hot" fusion with actinide targets [4]. Study of the dynamical process in fusion reactions, especially the nucleus-nucleus potential, is of great importance for the synthesis of superheavy elements. Experimentally, the fusion barrier distributions can be obtained directly from the measured fusion excitation functions, with which information on the nucleus-nucleus potential around the fusion barrier can be obtained. Figure 1(a) shows the nucleus-nucleus potential calculated with different models for $^{40}Ca + ^{40}Ca$. We can see that the obtained barrier heights with different models are close to each other and all of them are comparable to the extracted mean barrier height, while the calculated nucleus-nucleus potentials at short distances are quite different with different models. It is known that adiabatic and diabatic approximations lead to different nucleus-nucleus potentials, especially at short distances, and thus to different fusion paths and different mechanisms of fusion reactions. Both approximations are frequently applied to study of the synthesis of superheavy nuclei [1,10]. To understand the fusion mechanism of a heavy system, it is important and necessary to study the nucleus-nucleus potential at short distances, with which one can obtain information on the fusion path and the formation probability of a dinuclear system in reactions leading to superheavy nuclei.

For description of heavy-ion fusion reactions, some theoretical models have been developed. The fusion coupled-channel model is a powerful tool for calculation of the fusion excitation function and investigation of the influence of nuclear structure effects on fusion cross sections [11–13]. Some microscopic dynamics models, such as the time-dependent Hartree-Fock (TDHF) model [14,15] and the improved quantum molecular dynamics (ImQMD) model [16,17], are widely applied to study of the dynamical behavior of the fusion process. The ImQMD model is a semiclassical microscopic dynamics model and is successfully used for intermediate-energy heavy-ion collisions and for heavy-ion collisions at energies near the Coulomb barrier [16–19]. In the ImQMD model dynamical effects, such as dynamical deformation and neck formation, are microscopically and self-consistently taken into account. Recently, the model has been applied to the study of the dynamical barrier of a heavy system [20], of mass parameters [21], and of the strongly damped process of $^{238}U + ^{238}U$ [22,23]. In this paper we carefully investigate the kinetic energies of nuclei based on the extended Thomas-Fermi (ETF) approximation with which the dynamical fusion barrier is accurately obtained. The paper is organized as follows: In Sec. II, the ImQMD model is briefly introduced. In Sec. III, some calculated results on the kinetic energies of nuclei and the nucleus-nucleus potential for $^{40}Ca + ^{40}Ca$, $^{48}Ca + ^{208}Pb$, and $^{126}Sn + ^{130}Te$ are presented. Finally, a summary is given in Sec. IV.

II. THE IMPROVED QUANTUM MOLECULAR DYNAMICS MODEL

In the ImQMD model, as in the original QMD model [24], each nucleon is represented by a coherent state of a Gaussian wave packet. Through a Wigner transformation, the one-body phase-space distribution function for N-distinguishable particles is obtained (see Refs. [24] and [16] for details). The density distribution function ρ of a system reads

$$\rho(\mathbf{r}) = \sum_i \frac{1}{(2\pi\sigma_r^2)^{3/2}} \exp\left[-\frac{(\mathbf{r}-\mathbf{r}_i)^2}{2\sigma_r^2}\right], \tag{1}$$

where σ_r represents the spatial spread of the wave packet. The propagation of nucleons is governed by Hamiltonian equations of motion under the self-consistently generated mean field:

$$\dot{\mathbf{r}}_i = \frac{\partial H}{\partial \mathbf{p}_i}, \quad \dot{\mathbf{p}}_i = -\frac{\partial H}{\partial \mathbf{r}_i}, \tag{2}$$

*Corresponding author: wangning@gxnu.edu.cn

 ©2010 The American Physical Society

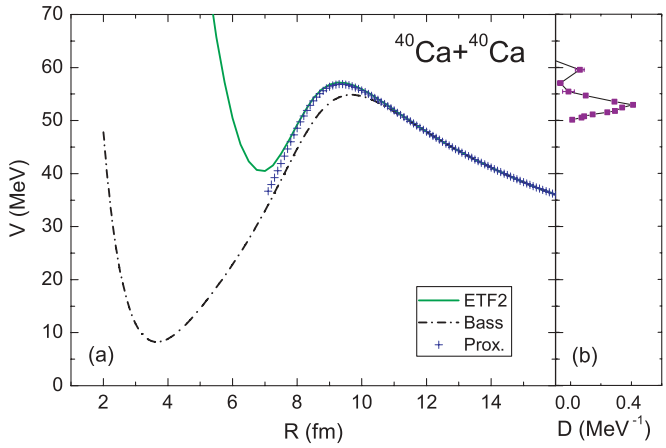

FIG. 1. (Color online) (a) The nucleus-nucleus potential as a function of the center-to-center distance R between two nuclei for the reaction ^{40}Ca + ^{40}Ca. The solid curve denotes the results from the Skyrme energy density functional together with the extended Thomas-Fermi (ETF2) approximation [5]. The dash-dotted curve and the plus signs denote the Bass potential [6] and the proximity potential [7], respectively. (b) The fusion barrier distribution extracted from the measured fusion excitation function [8] (see Eq. (9) of Ref. [9]).

where $\mathbf{r}_i$ and $\mathbf{p}_i$ are the center of the ith wave packet in the coordinate and momentum space, respectively. The Hamiltonian H consists of the kinetic energy and the effective interaction potential energy:

$$H = T + U, \tag{3}$$

$$T = \sum_i \frac{\mathbf{p}_i^2}{2m}. \tag{4}$$

The effective interaction potential energy includes the nuclear interaction potential energy and the Coulomb interaction potential energy,

$$U = U_{\rm loc} + U_{\rm Coul}, \tag{5}$$

with

$$U_{\rm loc} = \int V_{\rm loc}(\mathbf{r}) d\mathbf{r}, \tag{6}$$

where $V_{\rm loc}(\mathbf{r})$ is the potential energy density that is obtained by the effective Skyrme interaction and taken to be the same as that in Ref. [17]:

$$V_{\rm loc} = \frac{\alpha}{2}\frac{\rho^2}{\rho_0} + \frac{\beta}{\gamma+1}\frac{\rho^{\gamma+1}}{\rho_0^{\gamma}} + \frac{g_{\rm sur}}{2\rho_0}(\nabla\rho)^2 + g_\tau\frac{\rho^{\eta+1}}{\rho_0^{\eta}} + \frac{C_s}{2\rho_0}[\rho^2 - \kappa_s(\nabla\rho)^2]\delta^2, \tag{7}$$

where $\delta = (\rho_n - \rho_p)/(\rho_n + \rho_p)$ is the isospin asymmetry. Inserting expression (1) together with Eq. (7) into Eq. (6), we obtain the interaction potential energy:

$$U_{\rm loc} = \frac{\alpha}{2}\sum_i \frac{\rho_i}{\rho_0} + \frac{\beta}{\gamma+1}\sum_i\left(\frac{\rho_i}{\rho_0}\right)^{\gamma} + \frac{g_0}{2}\sum_i\sum_{j\neq i} f_s\frac{\rho_{ij}}{\rho_0} + g_\tau\sum_i\left(\frac{\rho_i}{\rho_0}\right)^{\eta} + \frac{C_s}{2}\sum_i\sum_{j\neq i} t_i t_j\frac{\rho_{ij}}{\rho_0}(1-\kappa_s f_s), \tag{8}$$

TABLE I. Parameter set IQ2.

α (MeV)	−356
β (MeV)	303
γ	7/6
g_0 (MeV fm^2)	7.0
g_τ (MeV)	12.5
η	2/3
C_s (MeV)	32.0
κ_s (fm^2)	0.08
ρ_0 (fm^{-3})	0.165

where

$$\rho_i = \sum_{j\neq i}\rho_{ij} = \sum_{j\neq i}\frac{1}{(4\pi\sigma_r^2)^{3/2}}\exp\left[-\frac{(\mathbf{r}_i-\mathbf{r}_j)^2}{4\sigma_r^2}\right], \tag{9}$$

$$f_s = \frac{3}{2\sigma_r^2} - \left(\frac{\mathbf{r}_i-\mathbf{r}_j}{2\sigma_r^2}\right)^2, \tag{10}$$

and $t_i = 1$ for protons and -1 for neutrons, respectively. The parameter set IQ2 [18] (see Table I) is adopted in this work. The Coulomb energy is written as the sum of the direct and the exchange contribution, with the latter being taken into account in the Slater approximation [25,26],

$$U_{\rm Coul} = \frac{e^2}{2}\int\frac{\rho_p(\mathbf{r})\rho_p(\mathbf{r}')}{|\mathbf{r}-\mathbf{r}'|}d\mathbf{r}d\mathbf{r}' - e^2\frac{3}{4}\left(\frac{3}{\pi}\right)^{1/3}\int\rho_p^{4/3}d\mathbf{r}. \tag{11}$$

To describe the fermionic nature of the N-body system and to improve the stability of an individual nucleus, the phase-space occupation constraint method [27] and the system-size-dependent wave-packet width $\sigma_r = 0.09A^{1/3} + 0.88$ fm [18] are adopted. The phase-space occupation constraint is an effective approach to improve the momentum distribution of the nuclear system [16,27]. In this approach, the phase-space occupation number of each particle is checked at each time step. If the phase-space occupation number is larger than 1 for particle i, that is, $\bar{f}_i > 1$, the momentum of particle i is randomly changed by a series of two-body elastic scatterings between i and its partner that guarantee that the total momentum and total kinetic energy are conserved in the procedures. In the ImQMD model, the new sample for the momenta of the particles is constrained by the Pauli-blocking probability [27] as in the usual two-body collision process. Actually, the momenta of two particles obtained in this way influence the motion of particles in the system in not only this step but also the further steps. It is unknown whether the system will be in the most suitable motion path. In this work, we perform one further step; that is, we calculate the total energy of the system at step t and the total energy $E(t+\Delta t)$ at the next time step $(t+\Delta t)$ simultaneously. If the value of $E(t+\Delta t)$ obviously deviates from that of $E(t)$, the two-body elastic scattering procedure is re-executed. The number of times to re-execute the procedure is small (zero to four) at each time step for fusion reactions. This additional constraint can further improve the stability of an individual nucleus (reducing the spurious emission of nucleons) and

is helpful for study of the formation process of compound nuclei, which lasts several thousand fm/c or longer. We have checked that the total energy of the system is well conserved for thousands of fm/c with this new procedure.

III. RESULTS

In this section we first study the kinetic energies of a series of nuclei, then calculate the nucleus-nucleus potential in fusion reactions based on the ETF approximation.

A. Kinetic energies of nuclei

We first study the kinetic energy of a series of nuclei in the ground state from ^{16}O to ^{259}No. Based on the extended Thomas-Fermi approximation [28], the kinetic energy of a free Fermi gas can be expressed as

$$E_k = \frac{\hbar^2}{2m}\int \tau(\mathbf{r})d\mathbf{r} = c_k\langle\rho\rangle^{2/3} + \frac{\hbar^2}{2m}\frac{1}{36}\int\frac{(\nabla\rho)^2}{\rho}d\mathbf{r} + \cdots, \tag{12}$$

with the kinetic energy density $\tau(\mathbf{r})$ and the coefficient $c_k = (\hbar^2/2m)(3/5)(3\pi^2/2)^{2/3}$. With the help of the ETF form of the kinetic energy for a Fermi gas system in Eq. (12), we express the kinetic energy of an individual nucleus in the ImQMD model as

$$E_k^{\mathrm{ETF}} \simeq c_0\sum_i \rho_i^{2/3} + \frac{c_1}{\sum\rho_i}\sum_{i,j\neq i} f_s\rho_{ij} + c_2 N, \tag{13}$$

with $c_0 = 41.2$ MeV fm^2, $c_1 = 4.8$ MeV fm^2, and $c_2 = -1.0$ MeV for IQ2, which are determined by fitting the obtained kinetic energies of a series of nuclei with Eq. (4) (see Fig. 2). N is the particle number of the system under consideration. The expressions for ρ_i, ρ_{ij}, and f_s are given in Eqs. (9) and (10), respectively. The c_0 term in Eq. (13) represents the result of the Thomas-Fermi (TF) approximation [see the $\langle\rho\rangle^{2/3}$ term in Eq. (12)]. The other terms give the corrections from the finite-system effect.

Figure 2(a) shows the time average of the kinetic energy per particle for a series of nuclei. Here we take 100 events for each nucleus. Filled and open circles denote the results with Eq. (4) and with Eq. (13), which is based on the ETF approximation, respectively. Here ETF means that the form of Eq. (13) is roughly obtained according to the extended Thomas-Fermi approximation. The crosses in Fig. 2 denote the results with the TF approximation,

$$E_k^{\mathrm{TF}} \simeq c_0\sum_i \rho_i^{2/3}, \tag{14}$$

where the correction terms from the finite-system effect are not taken into account. Figure 2 shows that for light nuclei ($A < 50$), the calculated kinetic energies using the TF approximation are much smaller than the values using Eq. (4), while for heavy nuclei ($A > 150$), the results obtained with the TF approximation are slightly larger than those with Eq. (4). Only for intermediate nuclei the results are in agreement with each other. The kinetic energy calculated with the ETF approximation is in good agreement with the values from Eq. (4) except for very light nuclei. Figure 2 shows that the ETF approximation can reasonably well describe the kinetic energy for finite nuclei. The time evolution of the kinetic energies per particle for the nuclei ^{40}Ca, ^{90}Zr, and ^{208}Pb are shown in Fig. 2(b). The kinetic energies of these nuclei are well described by Eq. (13), based on the ETF approximation.

B. Nucleus-nucleus potential in fusion reactions

By using the ImQMD model, we can calculate the static and dynamical Coulomb barriers. In calculation of the static Coulomb barrier, which is based on the frozen density approximation, the initial density distribution of the projectile

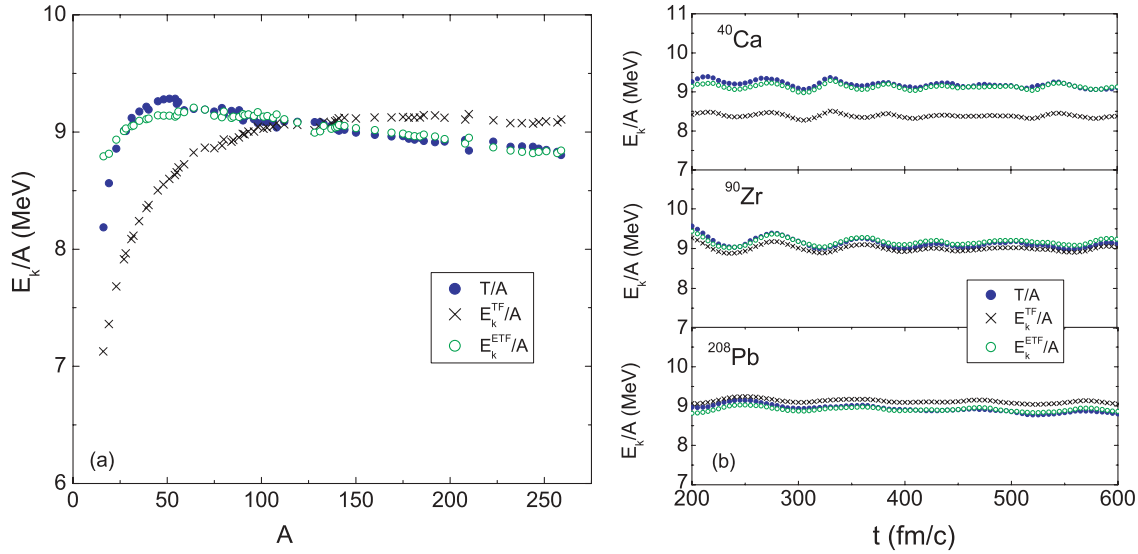

FIG. 2. (Color online) (a) Time average of the kinetic energy per particle for a series of nuclei. Filled circles, open circles, and crosses denote the results with Eqs. (4), (13), and (14), respectively. (b) Time evolution of the kinetic energy per particle for ^{40}Ca, ^{90}Zr, and ^{208}Pb.

and target is adopted. In calculation of the dynamical Coulomb barrier, the realistic density distribution of the system, which changes with time owing to the interaction between nucleons, is used. In this work, we concentrate on calculation of the dynamical fusion barrier. We study the dynamical nucleus-nucleus potential V based on the ETF approximation for the kinetic energy. According to the energy conservation, we have

$$E_{\rm c.m.} = T_R + V + E^* + T_{\rm oth}, \tag{15}$$

where $E_{\rm c.m.}$ is the incident center-of-mass energy; T_R is the relative motion kinetic energy of two colliding nuclei, which can be easily obtained in the ImQMD model, as the position and momentum of each nucleon can be followed at every time step; E^* is the excitation energy; and $T_{\rm oth}$ is other collective kinetic energy, such as neck vibration. When the projectile and target nuclei are well separated ($R \gg R_1 + R_2$), E^* and $T_{\rm oth}$ can be negligible, which has been checked by TDHF calculations [14,29], and the nucleus-nucleus potential is thus expressed as

$$V_1 = E_{\rm c.m.} - T_R, \tag{16}$$

where R_1 and R_2 are the charge radii of the projectile and the target nuclei, respectively, which are described by the empirical formula $R_i = 1.25A^{1/3}(1 - 0.2\frac{N-Z}{A})$, proposed in Ref. [30]. After the dinuclear system is formed ($R < R_1 + R_2$), the nucleus-nucleus potential may be described in a way like the entrance channel potential [31],

$$V_2 = E_{\rm tot}(R) - \bar{E}_1 - \bar{E}_2, \tag{17}$$

where $E_{\rm tot}(R)$ is the energy of the composite system, which is strongly dependent on the dynamical density distribution of the system obtained with the ImQMD model, and $\bar{E}_1$ and $\bar{E}_2$ are the time average of the energies of the projectile and target nuclei, respectively. Here, the values of $\bar{E}_1$ and $\bar{E}_2$ are obtained from the energies of the projectile(like) and target(like) nuclei in the region $R_T < R < R_T + 8$. $R_T = R_1 + R_2$ is the touching point. R is the relative distance between the two nuclei, which is a function of time. In the calculation of $E_{\rm tot}(R)$, $\bar{E}_1$, and $\bar{E}_2$, Eq. (13), which is a function of the local density, is used for the description of the intrinsic kinetic energy of the system under consideration.

In this work, we write the nucleus-nucleus potential as a smooth function between V_1 and V_2:

$$V_b(R) = \tfrac{1}{2}{\rm erfc}(s)V_2 + \left[1 - \tfrac{1}{2}{\rm erfc}(s)\right]V_1, \tag{18}$$

where erfc(s) is the complementary error function and

$$s = \frac{R - R_T + \delta}{\Delta R}, \tag{19}$$

with $\delta = 1$ fm and $\Delta R = 2$ fm. The nucleus-nucleus potential obtained in Eq. (18) approaches V_1 with an increase in the separation distance between the two nuclei. On the contrary, $V_b(R)$ approaches V_2 with the formation of a dinuclear system and a decrease in the distance between the two nuclei. To study the dynamical nucleus-nucleus potential, we create 500 reaction events for head-on collision of ^{40}Ca + ^{40}Ca at several c.m. energies, ranging from $E_{\rm c.m.} = 52$ MeV to $E_{\rm c.m.} = 140$ MeV. For each event, we evolve the reaction system for a time of 700 fm/c. The distance between the projectile and the target at the initial time is set to 30 fm for this reaction. The scattering events at $t = 700$ fm/c are not involved in the calculation of the nucleus-nucleus potential. Figure 3 shows the dynamical nucleus-nucleus potentials obtained at different incident energies $E_{\rm c.m.}$. The corresponding density distributions at $E_{\rm c.m.} = 80$ MeV and different relative distances are also shown, in the insets at the bottom. Figure 4 shows the average fusion barrier height B for the reaction ^{40}Ca + ^{40}Ca at different $E_{\rm c.m.}$ values. Figures 3 and 4 show that the dynamical barriers depend on the

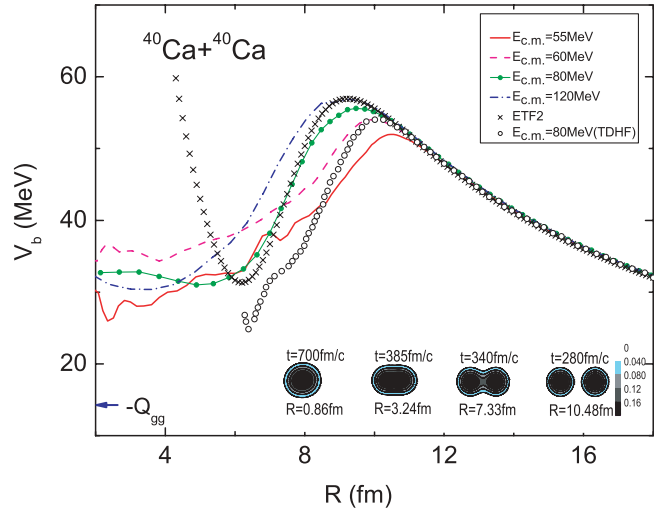

FIG. 3. (Color online) The dynamical nucleus-nucleus potential of ^{40}Ca + ^{40}Ca at different incident energies $E_{\rm c.m.}$. Crosses denote the entrance-channel potential with the Skyrme energy density functional approach [5], which is based on frozen density approximation. Open circles denote the results with TDHF [32] at $E_{\rm c.m.} = 80$ MeV. Insets: Density distributions for this reaction at $E_{\rm c.m.} = 80$ MeV and different relative distances.

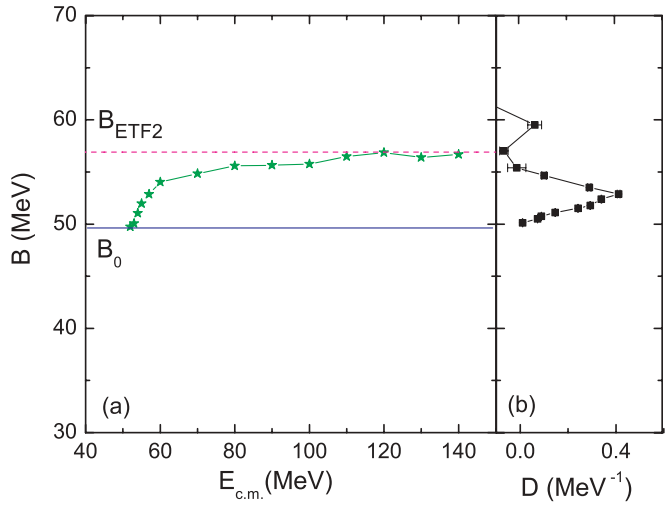

FIG. 4. (Color online) (a) Barrier height B for the reaction ^{40}Ca + ^{40}Ca at different incident energies $E_{\rm c.m.}$. Horizontal dashed and solid lines indicate the barrier height of the entrance-channel potential based on the frozen density approximation [5] and the lowest barrier B_0 extracted from the fusion excitation function [8], respectively. (b) Same as Fig. 1(b).

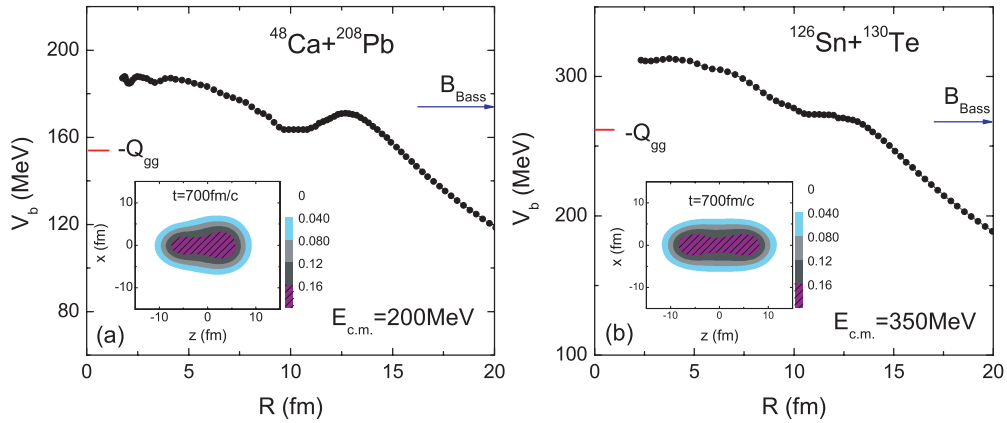

FIG. 5. (Color online) Dynamical nucleus-nucleus potentials for the reactions ^{48}Ca + ^{208}Pb and ^{126}Sn + ^{130}Te at incident energies $E_{\rm c.m.}$ = 200 MeV and $E_{\rm c.m.}$ = 350 MeV, respectively. The initial distance is set to 40 fm. Arrows denote the corresponding Bass barriers.

incident energies. At energies around the Coulomb barrier, the dynamical barrier increases rapidly with the incident energy. With a further increase in the incident energy, the dynamical barrier approaches the barrier height of the entrance-channel potential (56.9 MeV), which is obtained with the Skyrme energy density functional together with the frozen density approximation [5]. This trend was also found in Refs. [15] and [20]. When the incident energy decreases gradually down to $E_{\rm c.m.} = 55$ MeV, the height of the dynamical barrier falls to 52.0 MeV. At a lower incident energy, the height of the dynamical barrier approaches about 50 MeV, which is close to the height of the lowest barrier B_0 extracted from the fusion excitation function. In addition, it is encouraging that the barrier height and the depth of the fusion pocket obtained in this work are comparable to the results of the TDHF calculations [32]. The depth of the fusion pocket is about 25 MeV for this reaction system.

At very short distances between two nuclei, it is thought that the Q value of the fusion system may provide information on the nucleus-nucleus potential. One commonly defines the excitation energy for a reaction from the expression

$$-Q_{gg} = E_{\rm c.m.} - E^*, \tag{20}$$

where Q_{gg} is the mass difference between the two initial nuclei and the combined system in its ground state. From Eqs. (15) and (17), one finds that when the compound nucleus is well formed and the collective motion is negligible, one gets $V(R = 0) = -Q_{gg}$, which is the result of the adiabatic nucleus-nucleus potential [10]. For the reaction ^{40}Ca + ^{40}Ca, we get $-Q_{gg} = 14.3$ MeV. Actually, because expression (20) is correct relative to the ground state of the composite system, it does not accurately describe the excitation energy relative to other intermediate transition states formed during the collision [32], and the nucleus-nucleus potential obtained from the ImQMD model and the TDHF [32] at a short distance does not exactly reach the value $-Q_{gg}$, as the composite system formed during the collision is far from a ground state.

Using the same approach we studied the nucleus-nucleus potential for the reactions ^{48}Ca + ^{208}Pb and ^{126}Sn + ^{130}Te at energies above the Coulomb barrier. The corresponding values of $-Q_{gg}$ for these two reactions are 153.8 and 261.2 MeV, respectively. These two reactions lead to the same compound nucleus, ^{256}No. Figure 5 shows the calculated nucleus-nucleus potentials for these two reactions. The arrows denote the Bass barriers. From Fig. 5 we can see that the obtained barrier heights are close to the corresponding Bass barriers. The depth of the fusion pocket (about 7 MeV) for ^{48}Ca + ^{208}Pb becomes much shallower than that for ^{40}Ca + ^{40}Ca (about 25 MeV) and the fusion pocket for ^{126}Sn + ^{130}Te almost disappears, which indicates that quasifission could easily occur in the heavy fusion process, especially for more symmetric systems. Furthermore, we find that the nucleus-nucleus potentials for the reactions ^{48}Ca + ^{208}Pb and ^{126}Sn + ^{130}Te at short distances are much higher than the value of $-Q_{gg}$ and even higher than the Coulomb barrier, which is quite different from the case for ^{40}Ca + ^{40}Ca. These calculations indicate that (1) additional incident energy (so-called extra-push energy [2]) beyond the energy to overcome the Coulomb barrier may be required to form the compound nucleus for a heavy fusion system and (2) the process of nucleon transfer between the projectile(like) and the target(like) nuclei can last for a period of time, owing to the appearance of a fusion pocket in the dinuclear system, which is the basic assumption of the dinuclear system model [1]. To illustrate the fusion path, we also show the corresponding density distributions of the composite systems at $t = 700$ fm/c in the insets in Fig. 5. One can see that the corresponding compound nuclei are not well formed at $t = 700$ fm/c for these two heavy fusion systems. The strongly deformed composite systems, or so-called dinuclear systems, are formed at about $t = 350$ fm/c and can last hundreds or even thousands of fm/c for a heavy fusion system, which is quite different from the case for a light system such as ^{40}Ca + ^{40}Ca, in which the spherical composite system is well formed at $t = 700$ fm/c at incident energies above the Coulomb barrier (see Fig. 3). For ^{126}Sn + ^{130}Te, the composite system tends to undergo quasifission or fission. Figure 6 shows the capture cross sections of these two reactions. The open and filled circles in Fig. 6(a) denote the experimental data on ^{48}Ca + ^{208}Pb in Refs. [33] and [34], respectively. Solid curves denote the results of an empirical barrier distribution approach that is based on the Skyrme energy-density functional together with the ETF approximation [5,35]. Filled squares denote

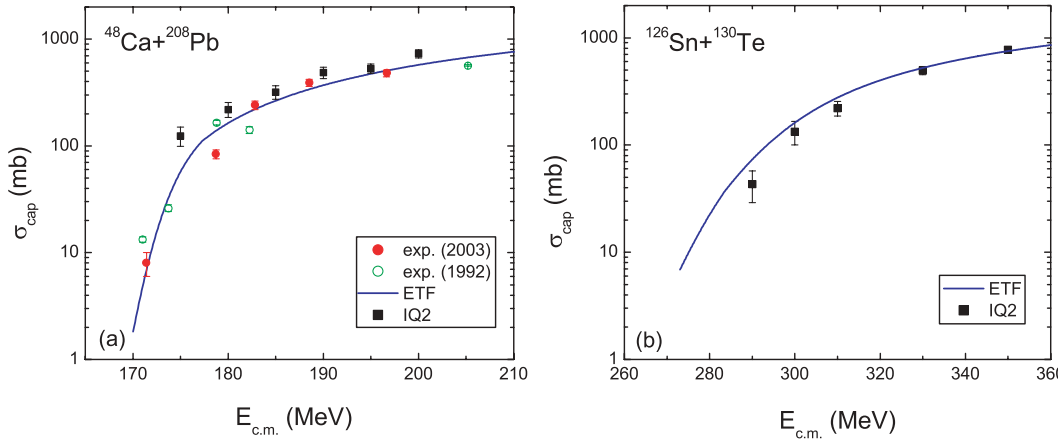

FIG. 6. (Color online) Capture cross sections for the reactions ^{48}Ca + ^{208}Pb and ^{126}Sn + ^{130}Te. Open and filled circles in (a) denote the experimental data for ^{48}Ca + ^{208}Pb [33,34]. Solid curves denote the results of an empirical barrier distribution approach proposed in Refs. [5] and [35]. Filled squares denote the results with the ImQMD model and error bars denote the corresponding statistical errors.

the results of the ImQMD model with IQ2, and error bars denote the corresponding statistical errors. For the reaction ^{48}Ca + ^{208}Pb, the experimental data at energies above the Coulomb barrier can be reproduced acceptably well by the ImQMD model. Because the ImQMD model has difficulties when dealing with shell effects, the capture cross sections of ^{48}Ca + ^{208}Pb at sub-barrier energies cannot be described well. For ^{126}Sn + ^{130}Te, the capture cross sections calculated with the ImQMD model are comparable to the results of the empirical barrier distribution approach.

IV. SUMMARY

In summary, the kinetic energies of a series of nuclei have been studied with the ImQMD model together with the ETF approximation, which gives accurate results for finite nuclear systems, especially for light and heavy nuclei. Furthermore, with the ETF approximation for the kinetic energies, we have studied the dynamical Coulomb barrier of the reaction ^{40}Ca + ^{40}Ca at different incident energies. The results show that the dynamical Coulomb barrier depends strongly on the incident energy. With an increase in incident energy, the dynamical Coulomb barrier increases gradually and approaches the entrance-channel potential, which is based on the frozen density approximation. The height of the dynamical Coulomb barrier decreases with a decrease in incident energy and approaches the lowest barrier extracted from the fusion excitation function. The behavior of the nucleus-nucleus potential at short distances for heavy systems is obviously different from that for light systems. For heavy fusion systems, the depth of the fusion pocket becomes much shallower and the nucleus-nucleus potential at short distances is higher than the adiabatic potential. The capture cross sections for ^{48}Ca + ^{208}Pb and ^{126}Sn + ^{130}Te have also been studied with the ImQMD model. The calculated results are comparable to the results of the empirical barrier distribution approach. A systematic study of heavy fusion systems, such as calculation of the potential energy surface of a composite system in the fusion process as a function of mass asymmetry and the distance between two nuclei, is in progress, with shell effects being taken into account.

ACKNOWLEDGMENTS

This work was supported by National Natural Science Foundation of China Grant Nos. 10875031, 10847004, 10979023, and 10979024 and Innovation Project of Guangxi Graduate Education Grant No. 2009106020702M36, and in part by National Basic Research Program of China No. 2007CB209900.

[1] G. G. Adamian *et al.*, Nucl. Phys. A **633**, 409 (1998).
[2] C. Shen, G. Kosenko, and Y. Abe, Phys. Rev. C **66**, 061602(R) (2002).
[3] S. Hofmann and G. Münzenberg, Rev. Mod. Phys. **72**, 733 (2000).
[4] Yu. Ts. Oganessian *et al.*, Phys. Rev. C **70**, 064609 (2004).
[5] M. Liu *et al.*, Nucl. Phys. A **768**, 80 (2006).
[6] R. Bass, *Nuclear Reactions with Heavy Ions* (Springer-Verlag, Berlin, Heidelberg, New York, 1980).
[7] W. D. Myers and W. J. Świątecki, Phys. Rev. C **62**, 044610 (2000).
[8] H. A. Aljuwair *et al.*, Phys. Rev. C **30**, 1223 (1984).
[9] N. Wang, Z. Li, and W. Scheid, J. Phys. G **34**, 1935 (2007).
[10] V. Zagrebaev *et al.*, Phys. Part. Nucl. **38**, 469 (2007).
[11] K. Hagino, N. Rowley, and A. T. Kruppa, Comput. Phys. Commun. **123**, 143 (1999).
[12] T. Ichikawa, K. Hagino, and A. Iwamoto, Phys. Rev. C **75**, 057603 (2007).
[13] H. Esbensen and Ş. Mişicu, Phys. Rev. C **76**, 054609 (2007).
[14] A. S. Umar and V. E. Oberacker, Phys. Rev. C **74**, 021601(R) (2006).
[15] K. Washiyama and D. Lacroix, Phys. Rev. C **78**, 024610 (2008).

[16] N. Wang, Z. Li, and X. Wu, Phys. Rev. C **65**, 064608 (2002).
[17] N. Wang, Z. Li, X. Wu, J. Tian, Y. X. Zhang, and M. Liu, Phys. Rev. C **69**, 034608 (2004).
[18] N. Wang *et al.*, Mod. Phys. Lett. A **20**, 2619 (2005).
[19] Y. Zhang *et al.*, Phys. Lett. B **664**, 145 (2008).
[20] J. Tian, X. Li, X. Wu, Z. Li, and S. W. Yan, Eur. Phys. J. A **42**, 105 (2009).
[21] K. Zhao, Z. Li, X. Wu, and Z. Zhao, Phys. Rev. C **79**, 024614 (2009).
[22] J. Tian, X. Wu, K. Zhao, Y. Zhang, and Z. Li, Phys. Rev. C **77**, 064603 (2008).
[23] K. Zhao, X. Wu, and Z. Li, Phys. Rev. C **80**, 054607 (2009).
[24] J. Aichelin, Phys. Rep. **202**, 233 (1991).
[25] J. C. Slater, Phys. Rev. **81**, 385 (1951).
[26] J. Bartel and K. Bencheikh, Eur. Phys. J. A **14**, 179 (2002).
[27] M. Papa, T. Maruyama, and A. Bonasera, Phys. Rev. C **64**, 024612 (2001).
[28] M. Brack, C. Guet, and H. B. Hakanson, Phys. Rep. **123**, 275 (1985).
[29] S. E. Koonin *et al.*, Phys. Rev. C **15**, 1359 (1977).
[30] B. Nerlo-Pomorska and K. Pomorski, Z. Phys. A **348**, 169 (1994).
[31] V. Yu. Denisov and W. Nörenberg, Eur. Phys. J. A **15**, 375 (2002).
[32] A. S. Umar *et al.*, Phys. Rev. C **80**, 041601(R) (2009).
[33] E. V. Prokhorova *et al.*, arXiv:nucl-ex/0309021.
[34] A. J. Pacheco *et al.*, Phys. Rev. C **45**, 2861 (1992).
[35] N. Wang, X. Wu, Z. Li, M. Liu, and W. Scheid, Phys. Rev. C **74**, 044604 (2006).